

Fig. 7. The nuclear polarization  $f_N$  as a function of magnetic field  $H$  at  $S/R=0.514$  as calculated from the measured  $f_e$  and  $T$ .

The measurement of the magnetic moment-entropy curve over a range of magnetic fields is especially con-

venient in that the same data are useful in  $\gamma$ -ray heating measurements and in experiments based on Eq. (5).

#### Calculation of $f_N$ from Measured $f_e$ and $T$

These measured values of  $f_e$  and  $T$  may now be substituted in Eq. (1) to obtain the nuclear polarization  $f_N$  as a function of  $H_e$  at  $S/R=0.514$ . This result is plotted in Fig. 7. It is seen that a maximum polarization  $f_N=0.207$  is obtainable at a final field of 1300 gauss, and that the final fields (2260–2350 gauss) used in the nuclear polarization experiments<sup>1</sup> correspond to  $f_N=0.165$  to 0.170 for the initial polarization of the nuclei.

#### ACKNOWLEDGMENTS

We wish to express our appreciation to Dr. M. E. Rose, Dr. S. Bernstein, Dr. C. P. Stanford, and Dr. T. E. Stephenson for many interesting discussions, and to Mr. J. B. Capehart for technical assistance.

## Resonant States of $Mg^{24}$ Excited by Protons on Sodium\*

P. H. STELSON† AND W. M. PRESTON‡

Massachusetts Institute of Technology, Cambridge, Massachusetts

(Received April 8, 1954)

The gamma-ray yield from sodium was measured as a function of proton bombarding energy over the range 1.0 to 2.5 Mev using resolutions of 2.5 keV or better. In addition, the yield of  $\alpha$  particles produced by the  $Na^{23}(p,\alpha)Ne^{20}$  reaction and leading to the ground state of the residual nucleus was measured for proton energies of 1.0 to 2.2 Mev, with a resolution of 10 keV. Fifty-two resonances were observed in all. The resulting average level spacing is 28 keV at a mean excitation energy of 13.5 MeV in the compound nucleus  $Mg^{24}$ . The resonances vary in natural width from less than 0.3 keV to 50 keV. The energy spectra of the gamma rays from a number of resonances were investigated with a single-crystal NaI(Tl) scintillation spectrometer. The spectra consist mainly of two gamma rays, with energies of  $0.45 \pm 0.01$  and  $1.63 \pm 0.02$  MeV. These are interpreted as transitions from the first excited states of the residual nuclei formed by the reactions  $Na^{23}(p,p')Na^{23}$  and  $Na^{23}(p,\alpha')Ne^{20}$ , respectively.

### INTRODUCTION

THE interaction of fast protons with sodium nuclei was first observed by the detection of gamma radiation.<sup>1</sup> Curran and Strothers<sup>2</sup> studied the gamma-ray yield as a function of proton bombarding energy below 1 MeV and identified several maxima characteristic of resonance reactions. Measurements of the secondary electron absorption showed that many of the gamma rays were of high energy and hence presumably due to the radiative capture process. Burling<sup>3</sup>

confirmed and more clearly resolved the resonances below 1 MeV and found a number of additional resonances in the region 1.0 to 1.9 MeV. However, even with the improved resolution of 10 to 25 keV, Burling concluded that the measured half-widths of the resonances were largely experimental in origin. Tangen,<sup>4</sup> using better resolution, found three new resonances in the low-energy region 0.25 to 0.50 MeV.

It was recognized that the  $(p,\alpha)$  reaction is energetically possible and might give rise to gamma radiation of lower energy characteristic of the low-lying excited levels of the residual  $Ne^{20}$  nucleus. Curran and Strothers showed that this was not a prominent mode of decay for resonances below 1-MeV proton energy. Burling did not undertake energy measurements of the gamma radiation. As one proceeds to higher proton energies,

\* This work was jointly supported by the Bureau of Ships and the U. S. Office of Naval Research.

† Now at Oak Ridge National Laboratory, Oak Ridge, Tennessee.

‡ Now at Harvard University, Cambridge, Massachusetts.

<sup>1</sup> Herb, Kerst, and McKibben, *Phys. Rev.* **51**, 691 (1937).

<sup>2</sup> S. C. Curran and J. E. Strothers, *Proc. Roy. Soc. (London)* **A172**, 72 (1939).

<sup>3</sup> R. L. Burling, *Phys. Rev.* **60**, 340 (1941).

<sup>4</sup> R. Tangen, *Kgl. Norske Videnskab. Selskabs Skrifter* Nr. 1 (1946).

the Coulomb barrier effect is reduced and one expects that eventually the states will decay predominantly by particle emission rather than by radiative capture. In the present case, for proton energies of less than 5 Mev, the gamma rays associated with particle emission are restricted to two reactions: those due to the de-excitation of Ne<sup>20</sup> produced by the (*p*, $\alpha$ ) reaction and those due to the de-excitation of Na<sup>23</sup> as the result of inelastic proton scattering.

Electrostatic generator techniques have advanced sufficiently to permit an increase in the energy homogeneity of the proton beam by a factor of 10 to 30 over that of the previous investigations. In addition, the advent of the scintillation crystal counter offers a highly efficient detector and one with which the energy spectrum of the gamma radiation can be rather simply determined. We therefore thought it worthwhile to undertake a new study of the gamma radiation from this reaction. We have also measured directly, by means of a particle detector, the relative yield as a function of proton energy of the  $\alpha$  particles which result from the reaction when Ne<sup>20</sup> is left in its ground state.

#### EXPERIMENTAL METHOD

##### The Proton Beam

The Rockefeller electrostatic generator<sup>5</sup> was used to produce the fast protons. This generator has an ion source of the radio-frequency type. The beam is analyzed by 90° deflection in a magnetic field which is stabilized and measured by a proton magnetic moment resonance device. The generator voltage is stabilized by a corona load which is driven by error signals produced by the proton beam at the exit slits of the analyzer. Proton beam currents of several microamperes were available in which the energy spread of the protons was approximately 0.02 percent. Experimental points taken at less than 0.01 percent difference in energy were reproducible over short intervals of time.

Energy measurements are based on the Li(*p*,*n*) threshold calibration point which is taken to be 1.8822 ± 0.0019 Mev as determined by Herb *et al.*<sup>6</sup> Over periods of several days, variations of about 0.1 percent in the voltage calibration have been observed. Hence, our absolute proton energies are subject to this uncertainty in addition to the 0.1 percent uncertainty of the calibration standard itself.

##### Gamma-Ray Counter and Target

The NaI crystal scintillation counter used for gamma-ray detection was constructed in the following way: a cylindrical NaI crystal 1½ in. in diameter and 1 in. long was ground smooth and solvent polished on one end. The crystal and a 5819 photomultiplier were placed in a thin-walled, airtight aluminum container

with the polished crystal surface butted against the photocathode. The crystal and photocathode surface were immersed in water-free Nujol for good optical coupling.

The 661-keV Cs<sup>137</sup> gamma ray was used to establish the energy calibration and energy resolution. The full-energy peak (the result of the photoelectric process or Compton scattering in which the scattered quantum is captured in the crystal) had a full width at half-maximum of 20 percent.<sup>7</sup>

For gamma-ray yield measurements, thin targets of sodium were prepared by evaporation of the metal in vacuum onto 10-mil tantalum disks. Target preparation was carried out in the target assembly of the generator. To reduce the carbon buildup effect and to prevent deterioration under proton bombardment the targets were rotated eccentrically and cooled by an air jet sprayed on the outside of the tantalum backing. The scintillation counter was located in the forward direction with respect to the proton beam and target; the distance from the target to the center of the NaI crystal was approximately 3 cm.

##### $\alpha$ -Particle Detector and Target

One expects in general from the target, in addition to the ground-state group of  $\alpha$  particles, (a) alphas of lower energy from transitions in which Ne<sup>20</sup> is left in an excited state; (b) elastically scattered protons from the target and the target backing, in relatively much larger numbers; and (c) inelastically scattered protons from the target or backing. Within the bombarding proton energy range of 1.0 to 2.5 Mev, it proved practical to detect separately the  $\alpha$ -particle group associated with transitions to the ground state by using a special gas-filled proportional counter and pulse-height discrimination.

A thin nickel foil window, 0.4 air cm thick and 0.1 cm<sup>2</sup> area, was mounted on the side of a cylindrical counter of 1-in. diameter and 4-in. length. The particles pass through the window and traverse the counter perpendicular to its axis so that the path length in the gas is about 1 in. The counter was mounted in a small scattering chamber and placed so as to detect particles emerging from the target at 135° to the forward direction. The window was approximately 3 cm from the target. The counter center wire was 5-mil tungsten. A gas mixture of 90-percent argon—10-percent CO<sub>2</sub> was used; the pressure was varied from ¼ to ½ atmosphere depending on the bombarding proton energy.

In operation, the gas pressure in the counter could be adjusted so that the ground-state group of alphas, at a given bombarding energy, was barely stopped before reaching the far wall of the counter. Then any other group of alphas, coming from transitions to

<sup>7</sup> Considerably better resolution (half-widths as low as 10 percent) has been reported for this type of counter. The quality of the photomultiplier probably limited our resolution. We were not able to undertake the testing of a large number of tubes.

<sup>5</sup> W. M. Preston and C. Goodman, Phys. Rev. **82**, 316 (1951).

<sup>6</sup> Herb, Snowdon, and Sala, Phys. Rev. **75**, 246 (1949).

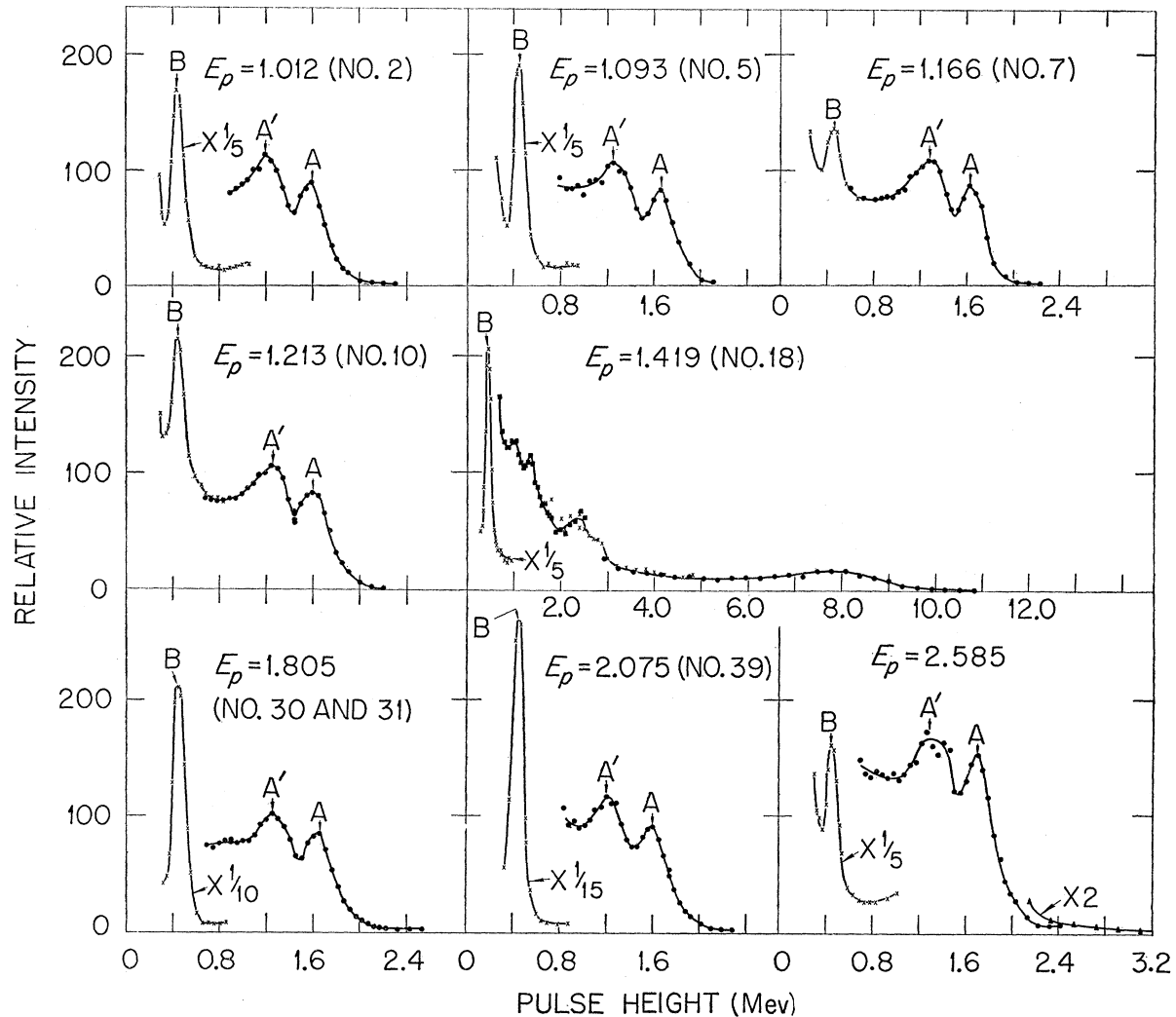


FIG. 1. Differential bias curves for a single-crystal NaI scintillation spectrometer, used to analyze the  $\gamma$  rays from sodium bombarded by protons, at various energies  $E_p$ . The abscissa scale is in Mev at the full-energy peak.

excited levels in  $\text{Ne}^{20}$ , would give smaller pulses. Protons of the same range, just able to cross the counter, gave substantially smaller pulses because of their smaller energy. Protons of greater range gave still smaller pulses because of their decreasing density of ionization along the effective path in the counter.

Although pulses from scattered protons were relatively small, their high intensity resulted in a serious pile-up problem. It was necessary to use thin Formvar target backings to reduce this to manageable proportions. The Formvar films are estimated to be roughly 25 micrograms/cm<sup>2</sup> thick. These were supported on small copper wire frames. The main drawback to the use of these thin backings is the limited beam current densities which they can take without disintegrating. We were forced to reduce the current to about 1/10 microampere which we dispersed over a target area of approximately 1 cm<sup>2</sup>. The targets were prepared by

evaporation of sodium metal, in vacuum, onto the backings. Surprisingly enough, the evaporation of a sodium layer onto the target backings did not drastically reduce the beam current capacity of the backings.

## EXPERIMENTAL RESULTS

### Gamma-Ray Energy Spectra

After preliminary yield curves had been run to locate resonances, the gamma-ray energy spectra at several resonances were measured. Some are shown in Fig. 1. With one exception, they exhibit a general similarity and a somewhat unexpected simplicity. Peaks *A* and *A'* may be attributed to the photoelectric and Compton electrons, respectively, from a gamma ray of  $1.63 \pm 0.02$ -Mev energy. Peak *B* is interpreted as the photoelectric peak of a gamma ray of  $0.45 \pm 0.01$ -Mev energy.

The processes which produce the two low-energy

gamma rays are revealed by the study of the energy level diagram of the relevant nuclei given in Fig. 2. The first excited state of  $Ne^{20}$  at 1.63 Mev has been observed in several different reactions.<sup>8</sup> The 1.63-Mev gamma ray therefore results from the  $(p,\alpha)$  reaction in which  $Ne^{20}$  is left in the first known excited state, designated as channel  $\alpha_1$ .

A level in  $Na^{23}$  at  $0.43 \pm 0.02$  Mev has been observed by Endt *et al.*<sup>9</sup> from a study of the  $Mg^{25}(d,\alpha)Na^{23}$  reaction. Recently, Donahue *et al.*<sup>10</sup> found this level by measuring the energy spectrum of protons inelastically scattered from sodium. It is thought, therefore, that the 0.45-Mev gamma ray is the result of the breakup of a compound state through channel  $p_1$ .

The existence of a second excited state in  $Ne^{20}$  at 2.2 Mev is questionable.<sup>8</sup> Even if this level exists and is excited through channel  $\alpha_2$ , the decay by gamma emission directly to the ground state is not observed. If the decay were by cascade to the 1.63-Mev level, one would expect a low-energy gamma ray of about 0.5 or 0.6 Mev and one might take this as an alternative explanation for the peak *B*. This is certainly not the case, however, since several resonances are observed for which there is an abundance of 0.45-Mev gamma rays but no detectable 1.63-Mev radiation. Recent work by Cox *et al.*<sup>11</sup> on the gamma rays excited by inelastic proton scattering on  $Ne^{20}$  shows no evidence of a level at 2.2 Mev.

At the highest proton energies the decay through channels  $p_2$  and  $\alpha_3$  is energetically possible, but it is probably suppressed because of the relatively low energy of the emerging particles. The gamma-ray spectra taken at the higher proton energies give no evidence for decay by these channels. However, decay by channel  $p_2$  might escape notice if it is predominantly by cascade to the 0.45-Mev level, since this would give rise to a 1.63-Mev gamma ray which cannot be distinguished from the 1.63-Mev gamma ray from  $Ne^{20}$ .

The spectra suggest that the radiative capture process is generally much less probable than particle emission for proton energies of 1 Mev and higher. Of the resonances studied, only the one at 1.419 Mev (No. 18) shows a fairly large intensity of high-energy radiation.<sup>12</sup> A rough measure of the relative importance of the capture process for some of the other resonances is given by the following. From the counting rates and the variation of counter efficiency with energy it is estimated that the ratio of the number of gamma rays of 3 Mev or larger to the number of 1.63-Mev gamma rays is less than 0.04 for resonance 2, less than 0.02 for resonance 7, 10, 30, and 31.

<sup>8</sup> See review article of F. Ajzenberg and T. Lauritsen, *Revs. Modern Phys.* **24**, 321 (1952).

<sup>9</sup> Endt, Haffner, and Van Patter, *Phys. Rev.* **86**, 518 (1952).

<sup>10</sup> Donahue, Jones, McEllistrem, and Richards, *Phys. Rev.* **89**, 824 (1953).

<sup>11</sup> Cox, Loef, and Lind, *Phys. Rev.* **93**, 925 (1954).

<sup>12</sup> The energy scale is not very accurate at the high energies since it is based on the low-energy  $Cs^{137}$  gamma ray.

Although the capture gamma-ray intensity may be small compared to that of the low-energy gamma rays which follow particle emission, it is not expected to be zero. Teener *et al.*<sup>13</sup> have measured the gamma-ray energy spectra by taking pictures of the pulses from a NaI crystal counter, displayed on the face of an oscilloscope. This is a technique well suited to the detection of weak, high-energy radiation. They observed high-energy gamma rays at a number of resonances.

### Gamma-Ray Yield Curves

The  $\gamma$ -ray yield from a thin sodium target is plotted in Fig. 3 as a function of the energy of the bombarding protons. The output of the linear amplifier, which followed the scintillation counter, was fed into two discriminator circuits in parallel. The first circuit was biased at 0.75 Mev, the second at 0.3 Mev.<sup>14</sup> The first circuit counting rate, corrected for background with zero proton beam, is plotted as a solid line Fig. 3; it is a measure of the number of  $\gamma$  rays above approximately 0.75 Mev. From the sample spectra shown in Fig. 1,<sup>15</sup> we can conclude that at most resonances there are only two  $\gamma$  rays present with appreciable intensities above 0.3 Mev, namely the 1.63- and 0.45-Mev rays. To this extent, the solid curve represents the yield of 1.63-Mev  $\gamma$  rays and therefore the yield of the  $Na^{23}(p,\alpha)Ne^{20*}$  reaction through channel  $\alpha_1$ . The curve has not been corrected for a background of  $\gamma$  rays produced by protons in the tantalum target backing. As shown by the inset in Fig. 4, this correction increases smoothly with  $E_p$  and is still small at the upper limit of the energy range investigated.

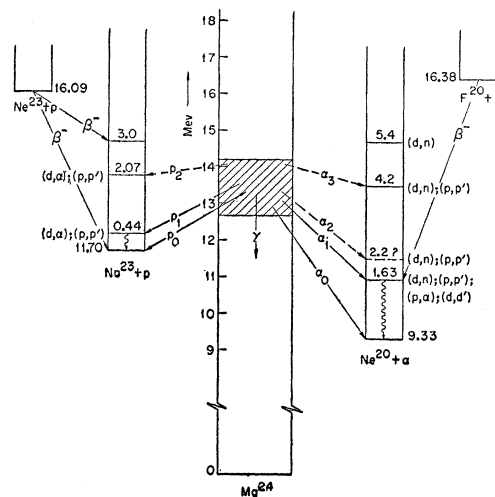


FIG. 2. Simplified energy level diagram for  $Mg^{24}$  and neighboring nuclei.

<sup>13</sup> Teener, Seagondollar, and Krone, *Phys. Rev.* **93**, 1035 (1954) and private communication.

<sup>14</sup> More accurately stated, the first discriminator bias was set to pass all pulses larger than the most probable pulse height due to photoelectrons from a 0.75-Mev  $\gamma$  ray.

<sup>15</sup> It did not seem worth while to measure the  $\gamma$ -ray spectra at all resonances.

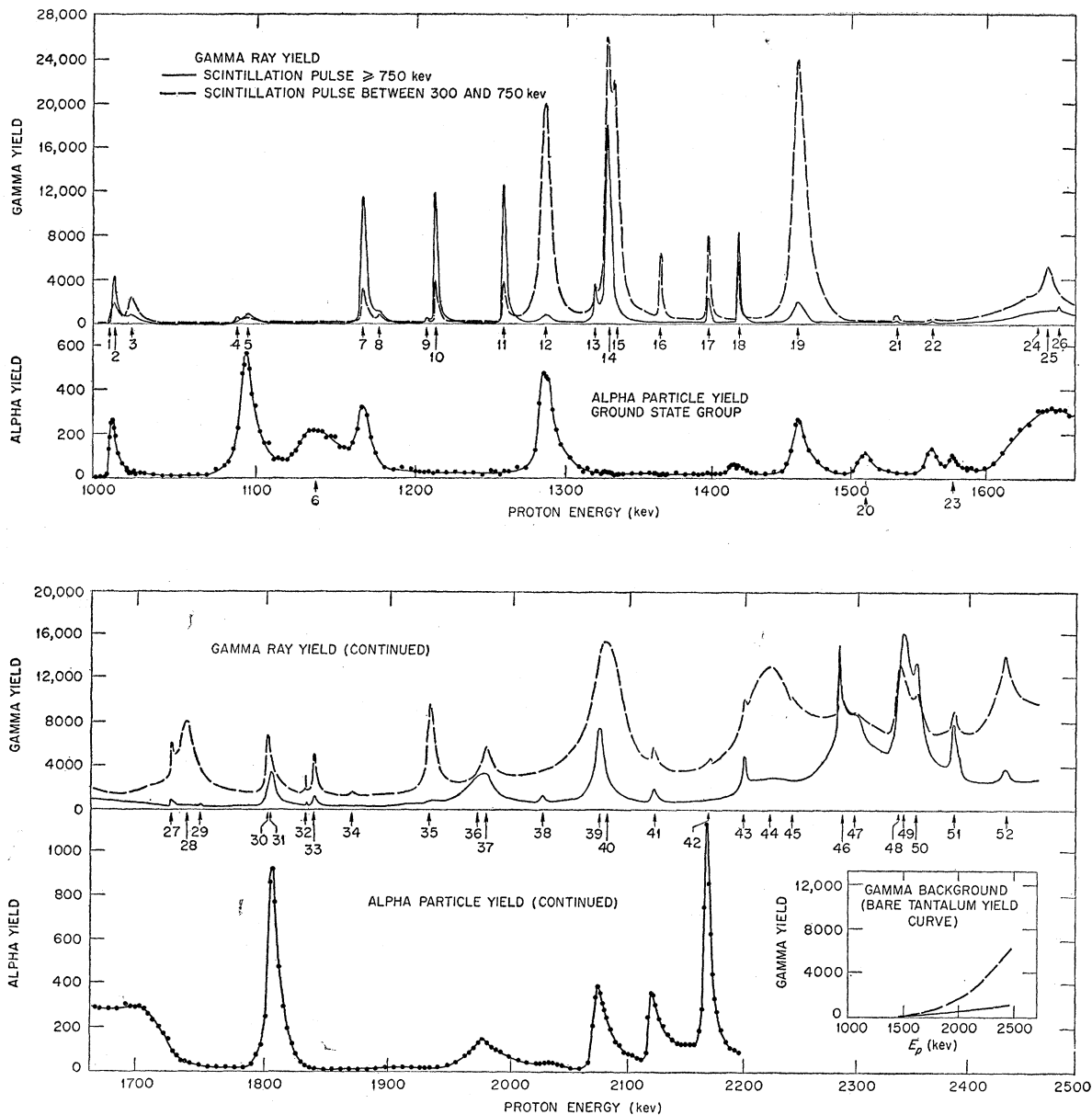


FIG. 3. Yield curves showing resonances in the yields of  $\gamma$  rays and  $\alpha$  particles from sodium bombarded by protons. The  $\gamma$ -ray yield is analyzed into two components: the solid curve represents pulses from the scintillation counter corresponding to energies greater than 750 keV, the dashed curve to pulses between 300 and 750 keV. These are interpreted as due largely to the reactions  $\text{Na}^{23}(p,\alpha)\text{Ne}^{20*}$  and  $\text{Na}^{23}(p,p')\text{Na}^{23*}$ , respectively. The ordinates for the solid and dashed curves are counts/40 microcoulombs and counts/20 microcoulombs, respectively. The  $\alpha$ -particle yield curves, taken with a gas-filled proportional counter, show the relative yield (counts/2 microcoulombs) from the reaction  $\text{Na}^{23}(p,\alpha)\text{Ne}^{20}$  leading to the ground state. The insert shows the yield of  $\gamma$  rays from the bare tantalum target backing.

The dashed curve in Fig. 3 is the difference in the counting rates in the two discriminator circuits. It may be interpreted as roughly proportional to the yield of 0.45-Mev  $\gamma$  rays, and hence of the reaction  $\text{Na}^{23}(p,p')\text{Na}^{23*}$  through channel  $p_1$ . The correction for background from the tantalum backing, shown again in the insert of Fig. 3, is considerably larger in this lower range of pulse heights.<sup>16</sup>

<sup>16</sup> A further correction arises from the fact that some pulses would be recorded in this channel, even from a pure source of

Experimental points were spaced so closely that they cannot be shown in Fig. 3. Figure 4 shows two typical 1.63-Mev  $\gamma$  rays, due to the low-energy tail of the pulse-height distribution. That this correction is relatively small can be seen as follows. At resonance No. 7 in Fig. 3, the yield of pulses in the nominally  $p_1$  channel is approximately one-half the yield above 750 keV. (The figure shows the ratio as one-fourth since the ordinates for the dotted curve and solid curve are counts/20 microcoulombs and counts/40 microcoulombs, respectively.) In Fig. 1, peak B of No. 7 is still pronounced, which indicates that a large share of these pulses in the  $p_1$  channel really come from the 0.45-Mev  $\gamma$  rays.

sections of the  $\gamma$ -ray yield curve on a much enlarged scale. Of the resonances shown in Fig. 4, Nos. 13, 14, 17, 18, 32, and 33 coincide exactly in both reactions,  $p_1$  and  $\alpha_1$ . Nos. 15 and 16 show no trace in the  $\alpha_1$  reaction. Nos. 30 and 31 are distinct; the former is due largely to the  $p_1$  channel, the latter to the  $\alpha_1$ .

Most of the  $\gamma$ -ray yield curves of Fig. 3 were taken with targets of about 2.5-keV stopping power for 1-MeV protons, and less at higher energies. The energy calibration and the condition of the target were checked several times during the run by careful measurements of the contour of the sharp resonance No. 18, which has a natural width less than 300 eV, and of the counting rate at the peak of the broad resonance No. 19. In this way, carbon buildup on the target, loss of sodium by evaporation, or increase in effective thickness could be measured.

For reasons not well understood, it was impossible to produce uniform sodium targets with effective thickness  $\Gamma_t < 2$  keV (measured for protons at 1 MeV) which would remain unchanged for any length of time. With targets having  $\Gamma_t \sim 2$  keV, the natural width  $\Gamma$  of the broader resonances could be measured directly from the yield curves. We assume that  $\Gamma^2 = \Gamma_m^2 - \Gamma_t^2$ , where  $\Gamma_m$  is the measured width of a peak at half-maximum amplitude. This method is reasonably accurate for resonances having  $\Gamma \geq \Gamma_t$ .

The natural widths of a number of narrower resonances were measured by a modified "thick target" method. If an infinitely thick target is employed, the yield increases in a rounded step (see Fig. 5) in going over a resonance. If the total increase in yield is  $\Delta Y$ , and the bombarding-energy interval between the points  $\Delta Y/4$  and  $3\Delta Y/4$  is called  $\Gamma'$ , it can be shown<sup>17</sup> that  $\Gamma'$  measures directly the combined effect of the natural width  $\Gamma$  and any energy spread in the bombarding beam. An infinitely thick target is not very useful for

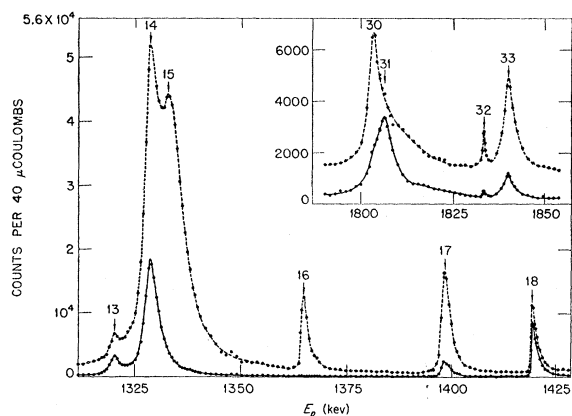


FIG. 4. Two portions of the  $\gamma$ -ray yield curves of Fig. 4 on an enlarged scale, showing the actual data points. The ordinates are counts/40 microcoulombs.

<sup>17</sup> Fowler, Lauritsen, and Lauritsen, *Revs. Modern Phys.* **20**, 236 (1948).

studying the width of a resonance which is preceded by many others at lower energies, since in traversing the resonance the yield will merely rise by a small increment over a large background. However, if a particular narrow resonance of natural width  $\Gamma$  is not too closely preceded by a neighboring resonance at lower energies, it is possible to use a target of intermediate thickness, say  $5\Gamma$ , which involves only small corrections over an infinitely thick target. At the same time, the yield from resonances at lower energies will be relatively small.

Figure 5 shows a number of such "rise curves." Of all resonances studied, No. 18 appeared to be the sharpest, with a  $\Gamma' = 0.31$  keV. The  $\gamma$ -ray spectrum for this resonance, Fig. 1, indicates that the capture radiation process competes favorably with particle emission. Since "radiation" widths are expected to be of the order of 0.01 keV or less, the natural width  $\Gamma$  of this resonance is probably substantially less than 0.31 keV. We can infer that the measured value of  $\Gamma' = 0.31$  keV is due largely to spread in energy of the incident proton beam. The indicated homogeneity of about one part in 4500 is somewhat better than that estimated from the geometry of the magnetic analyzer. This inferred value for the energy spread in the beam was used to correct other narrow measured half-widths, assuming that  $\Gamma^2 = (\Gamma')^2 - (0.31)^2$ .

In Table I we have listed the positions and estimated natural half-widths of all resonances measured. The positions have all been corrected for target thickness. They have been recorded to the nearest 0.1 keV, an accuracy justified only for computing the separations of neighboring resonances.

### Charged Particle Energy Spectra

Figure 6 shows several typical differential discriminator bias curves obtained with the charged particle detector previously described. From Fig. 2, the  $Q$  values for reactions going by channels  $\alpha_0$ ,  $\alpha_1$ ,  $p_0$ , and  $p_1$

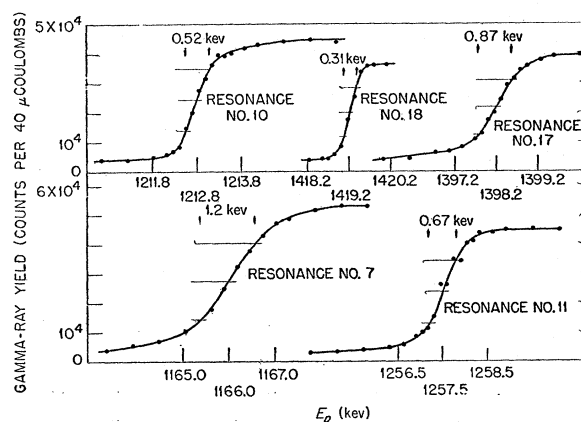


FIG. 5. Thick target  $\gamma$ -ray yield curves taken over five resonances, for protons of energy  $E_p$  on sodium. The indicated resonance widths are measured between the one-quarter and three-quarters rise points of thick-target yield curves.

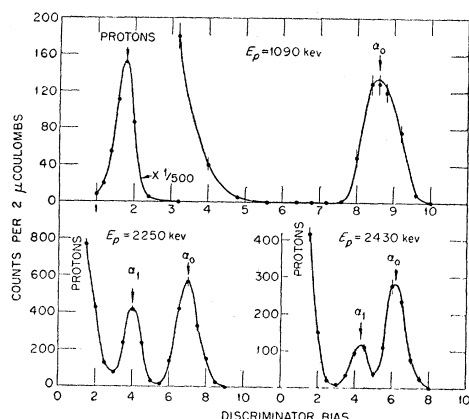


FIG. 6. Differential bias curves for a gas-filled proportional counter, used to detect scattered protons and  $\alpha$  particles from sodium bombarded by protons, at three different energies  $E_p$ .

are, respectively, 2.37, 0.74, 0.00, and  $-0.44$  Mev. For a bombarding proton energy of 1.090 Mev, the energies of the alphas and protons coming off at 135 degrees from the forward direction are computed to be  $E_{\alpha 0}=2.65$ ,  $E_{\alpha 1}=1.34$ ,  $E_{p 0}=0.94$ ,  $E_{p 1}=0.53$  Mev. Allowing for a loss of 0.40 cm air NTP in the nickel window and assuming a pressure in the counter of about 0.4 atmosphere, the energy loss of the various particles in the gas is estimated to be  $\Delta_{\alpha 0}=2.00$ ,  $\Delta_{\alpha 1}=0.46$ ,  $\Delta_{p 0}=0.42$ ,  $\Delta_{p 1}=1.18$  Mev. Inspection of the upper curve, Fig. 6, shows two peaks completely separated. They occur at energies with the ratio 4.7, in good agreement with that calculated for  $\Delta_{\alpha 0}/\Delta_{p 0}$ ; the high-energy peak can therefore be identified as arising from  $\alpha$  particles from transitions to the ground state of  $\text{Ne}^{20}$ . Alphas from channel  $\alpha_1$  and inelastically scattered protons, if present, are obscured by the large intensity of elastic protons.

In a similar manner, at a counter pressure of 0.56 atmosphere and a bombarding energy of 2.25 Mev, the calculated energy losses in the counter are  $\Delta_{\alpha 0}=2.6$ ,  $\Delta_{\alpha 1}=1.5$ ,  $\Delta_{p 0}=0.26$ , and  $\Delta_{p 1}=0.33$  Mev. In the lower left curve, Fig. 6, the two well-resolved peaks can be identified accordingly with the  $\alpha_0$  and  $\alpha_1$  channels. At a still higher bombarding energy, the different yields in the two channels is shown in the lower right-hand curve.

#### Ground-State Alpha-Particle Yield

The relative yield of  $\alpha$  particles from the  $\text{Na}^{23}(p,\alpha)$  reaction leading to the ground state of  $\text{Ne}^{20}$  is plotted in Fig. 3, from 1.0 to 2.2 Mev. In obtaining these data, the charged particle detector was used with a low cut-off discriminator. With information from several differential bias curves like those in Fig. 6, the bias was adjusted as the bombarding energy was increased so that only pulses from  $\alpha_0$ -channel alphas were counted. When necessary, the pressure in the counter was adjusted to get improved discrimination. The target thickness was about 10 kev; resolution and statistical

accuracy were considerably poorer than for the  $\gamma$ -ray yield curves.

In the  $\alpha_0$  yield curve, three new resonances appear, Nos. 6, 20, and 23, which are entirely absent from the  $\gamma$ -ray spectra. Conversely, a number of resonances which are strong in the  $\alpha_1$  or  $p_1$  channels are absent in the  $\alpha_0$  channel. These results are summarized in Table I.

#### DISCUSSION

Burling<sup>4</sup> identified 15 resonances in the bombarding proton energy range of 1.0 to 1.9 Mev; with the better

TABLE I. The columns headed  $\alpha_0$ ,  $H$  and  $L-H$  refer to the yield curves given in Fig. 3.  $H$  and  $L-H$  are the gamma-ray yield curves given by the solid and dotted lines, respectively. See the text for discussion of the interpretation of these yield curves in terms of the reaction channels  $\alpha_1$  and  $p_1$ . An  $x$  indicates that a measurable yield was obtained at a particular resonance.

No.	$E_r$	$\alpha_0$	$H$	$L-H$	$\Gamma$
1	1010.9			$x$	$\leq 0.5$
2	1012.3	$x$	$x$	$x$	$0.8 \pm 0.1$
3	1022.4		$x$	$x$	$6.6 \pm 0.5$
4	1087.1			$x$	$1.1 \pm 0.5$
5	1093.3	$x$	$x$	$x$	$7.9 \pm 0.5$
6	1137	$x$			$30 \pm 5$
7	1166.0	$x$	$x$	$x$	$1.2 \pm 0.1$
8	1176.2		$x$	$x$	$< 2.3$
9	1206.6		$x$	$x$	$0.3 \pm 0.1$
10	1212.8		$x$	$x$	$0.4 \pm 0.1$
11	1257.5		$x$	$x$	$0.6 \pm 0.1$
12	1287.5	$x$	$x$	$x$	$7.1 \pm 0.2$
13	1320.6		$x$	$x$	$2.1 \pm 0.5$
14	1328.7		$x$	$x$	$3.5 \pm 0.2$
15	1333.5			$x$	$6.7 \pm 0.2$
16	1364.9			$x$	$1.2 \pm 0.2$
17	1398.2		$x$	$x$	$0.8 \pm 0.1$
18	1419.2	$x$	$x$	$x$	$\leq 0.3 \pm 0.05$
19	1460.4	$x$	$x$	$x$	$9.8 \pm 0.2$
20	1511	$x$			$< 10$
21	1518.9		$x$	$x$	$3.2 \pm 0.5$
22	1558.2	$x$	$x$	$x$	$6.5 \pm 0.5$
23	1575	$x$			$< 10$
24	1637.9	$x$	$x$	$x$	$\sim 50$
25	1645.2			$x$	$\sim 8$
26	1653.1		$x$		$\sim 2$
27	1718.6		$x$	$x$	$2.0 \pm 0.5$
28	1737.3			$x$	$15.2 \pm 2$
29	1748.6		$x$		$\leq 1.0$
30	1802.3	$x$		$x$	$4 \pm 1$
31	1805.1	$x$	$x$		$6 \pm 1$
32	1832.4		$x$	$x$	$< 0.35$
33	1839.0		$x$	$x$	$3.2 \pm 0.2$
34	1870.2			$x$	$\sim 1$
35	1933.3		$x$	$x$	$6.9 \pm 0.5$
36	1976.1		$x$		$23 \pm 3$
37	1979.4	$x$		$x$	$9.5 \pm 1$
38	2026.8		$x$		$3.3 \pm 1$
39	2075.2	$x$	$x$		$8.7 \pm 0.5$
40	2080.1			$x$	$31 \pm 2$
41	2121.6	$x$	$x$	$x$	$4.8 \pm 0.5$
42	2169.5	$x$		$x$	$\sim 2$
43	2200.1		$x$	$x$	$3.5 \pm 0.5$
44	2222.6		$x$	$x$	$47 \pm 5$
45	2243.0			$x$	$\sim 2$
46	2284.3		$x$	$x$	$2.0 \pm 0.5$
47	2297.4		$x$	$x$	$\sim 28$
48	2340.0			$x$	$\sim 10$
49	2342.8		$x$		$\sim 14$
50	2354.4		$x$	$x$	$\sim 4$
51	2387.9	$x$	$x$	$x$	$4.9 \pm 0.5$
52	2435.9	$x$	$x$	$x$	$6.5 \pm 0.5$

resolution available to use, we have found 32 in the same interval. The average spacing for 52 resonances in the range 1.01 to 2.44 Mev is 28 kev. There is no indication of any decrease in the average level separation with increasing excitation energy.

The ground state of the even-even nucleus  $Ne^{20}$  is  $0^+$  (total angular momentum  $I=0$ , even parity); the first excited state is predicted to be  $2^+$ .<sup>18</sup> Seed<sup>19</sup> has confirmed this assignment. The ground state of  $Na^{23}$  predicted by shell theory is  $5/2^+$ ;<sup>20</sup> it is actually found to be  $3/2^+$ , so it is quite likely that the first excited state is  $5/2^+$ . With these assignments for the final states, the barrier penetrabilities can be computed for the decay of any excited state of  $Mg^{24}$  with given spin, parity, and excitation energy, by the channels  $\alpha_0$ ,  $\alpha_1$ ,  $p_0$ , and  $p_1$ . If the relative decay probability in different channels depended primarily on the penetrability factor, we might hope to make some headway in assigning spin and parity by a study of the experimental data summarized in Fig. 3 and Table I. Unfortunately, the factor in the decay probability which contains the matrix element for the transition<sup>21</sup> exhibits such wide variations<sup>22</sup> that detailed analysis seems unprofitable.

Since the  $\alpha$  particle has zero intrinsic spin, decay to the ground state of  $Ne^{20}$  in the channel  $\alpha_0$  can occur only from states in  $Mg^{24}$  belonging to the series  $0^+$ ,  $1^-$ ,  $2^+$ ,  $3^-$ , with the orbital angular momentum  $l$  of the  $\alpha$  particle necessarily equalling the spin  $I$  of the compound state (see Table II). This applies to sixteen of the 52 resonances listed in Table I. Three of these, Nos. 6, 20, and 23, could not be detected at all in the  $\alpha_1$  or  $p_1$  channels. It is likely that these latter are  $0^+$  states, which can decay by  $s$ -wave emission through  $\alpha_0$  but only by  $d$  waves ( $l=2$ ) in the  $\alpha_1$  and  $p_1$  channels. The

TABLE II. For states in  $Mg^{24}$  of total angular momentum and parity as indicated in the top line, the table shows the lowest permitted value of the orbital angular momentum,  $l$ , of a particle emitted in decay through four channels:  $p_0$  and  $p_1$ , proton emission to the ground state and first excited state of  $Na^{23}$ ;  $\alpha_0$  and  $\alpha_1$ ,  $\alpha$ -particle emission to the ground and first excited states of  $Ne^{20}$ , respectively.

State	$0^+$	$0^-$	$1^+$	$1^-$	$2^+$	$2^-$	$3^+$	$3^-$
Channel								
$p_0$	2	1	0	1	0	1	2	1
$p_1$	2	3	2	1	0	1	0	1
$\alpha_0$	0	—	—	1	2	—	—	3
$\alpha_1$	2	—	2	1	0	1	2	1

corresponding penetrabilities differ by a factor of over 1000, in the case of resonance No. 6.

Eight or nine resonances, of which Nos. 15 and 16 are the most striking examples, are not observed in either the  $\alpha_0$  or the  $\alpha_1$  channels. Decay from a  $0^-$  state is strictly forbidden by  $\alpha_0$  or  $\alpha_1$ , but must go by  $f$  wave in channel  $p_1$ ; an assignment of  $3^+$  is more reasonable for the resonances which are strong in  $p_1$ .

Another possible explanation for levels which do not decay by  $\alpha$  emission is found in the operation of isotopic spin selection rules. The proton has isotopic spin  $T=\frac{1}{2}$ . Combining with the lowest states of  $Na^{23}$ , which also have  $T=\frac{1}{2}$ , it can excite both singlet ( $T=0$ ) and triplet ( $T=1$ ) states in  $Mg^{24}$ . The positions of the ground states of the isobars  $F^{20}$ ,  $Ne^{20}$ , and  $Na^{20}$  show that the low-lying states of  $Ne^{20}$  have  $T=0$ . Hence only the singlet states of  $Mg^{24}$  are able to decay to  $Ne^{20}$  by emission of  $\alpha$  particles ( $T=0$ ). The positions of the isobars  $Na^{24}$ ,  $Mg^{24}$ ,  $Al^{24}$  indicate that the triplet states of  $Mg^{24}$  should first occur at excitation energies of 9 or 10 Mev; in the region here investigated, 3 or 4 Mev higher, the spacing of triplet levels is probably considerably larger than that of singlet levels.

In conclusion, we wish to thank Professor Clark Goodman and Mr. Clyde McClelland for their interest and help during the early stages of the work, and Mr. I. E. Slawson and Mr. D. C. Thompson for their invaluable assistance in the operation of the electrostatic generator.

<sup>18</sup> G. Scharff-Goldhaber, Phys. Rev. **90**, 587 (1953).

<sup>19</sup> J. Seed, Phil. Mag. **44**, 921 (1953).

<sup>20</sup> Mayer, Moszkowski, and Nordheim, Revs. Modern Phys. **23**, 315 (1951).

<sup>21</sup> Expressed sometimes in terms of an "effective level spacing"  $D$  or a "reduced level width"  $\gamma$ .

<sup>22</sup> Hinchev, Stelson, and Preston, Phys. Rev. **86**, 483 (1952).